Chapter 3

In-Silico investigation on repurposed drugs for Alzheimer's Disease

Chapter 3

3. In-Silico investigation on repurposed drugs for Alzheimer's disease

3.1 Introduction

The key toxic misfolded protein that causes Alzheimer's disease (AD), amyloid-beta, is mostly metabolized by the liver. This important function of the liver in AD is the subject of the current investigation. Through the hepatobiliary and enterohepatic circulations (EHC), we have developed a framework that formulates and integrates these two reciprocal transport processes of amyloid.

Our system analysis method demonstrates that by increasing the expression of the genes ATP-binding-cassette-transporter (ABCA1) and Stearoyl-CoA-desaturase (SCD), the activation of the liver X-receptor (LXR) can minimize amyloid-beta production. Additionally, by increasing the expression of the genes ATP-Binding-Cassette-Superfamily-G-member-2 (ABCG2) and multidrug-resistance protein-1 (MDR1), the activation of the pregnane-X-receptor (PXR) could enhance the clearance of amyloid-beta. We also identified an intestinal enterocyte entity with a receptor-like apical sodium-dependent bile acid transporter (ASBT) that exhibits affinity for amyloid-beta, indicating a potential pathway for absorption of amyloid-beta from intestinal contents into the systemic circulation.

Additionally, we have carried out protein-protein interactions to assess the amyloid-beta's binding affinity to these receptors. We also performed molecular docking and molecular dynamic simulation on certain repurposed drugs (rifampicin, 24-hydroxycholesterols, resveratrol, metformin and cilostazol) that can target the aforementioned receptors to increase fecal clearance of amyloid-beta, lessen amyloid-beta formation, and prevent reuptake of amyloid-beta from intestinal feces back into blood. In

addition, network pharmacology and synergism analysis were used to confirm our theory and, separately, find the medication combinations.

Network pharmacology, integrated pathway analysis, and gene-ontology analysis all support the modification of the aforementioned gene expression patterns. Furthermore, the ideal combination of the repurposed medications is determined by our neuropharmacological synergism study. Finally, the results of clinical trials analysed do support our conclusions regarding the candidate drugs.

3.2 Materials and methods

3.2.1 Molecular docking

3.2.1.1 Docking with amyloid-beta

GRAMM-X Protein-Protein Docking Web Server [49] was used to predict the binding sites of amyloid beta ([50]; PDB-id: 2 MXU) to the receptors ABCG2 homodimer, MDR1, LXR-beta, ASBT, and BSEP.

3.2.1.2 Docking with repurposed drugs

Protein-Data-Bank (www.rcsb.org) was used to retrieve the structures of the receptors PXR, LXR-β, ASBT, PDE-3B, and BSEP. The structures of the ligands (reprofiled drugs), rifampicin, 24-hydroxycholesterol, resveratrol, cilostazol, and metformin for the corresponding receptors were obtained from the PubChem compound database in SDF format. Using the PyRx tool, the ligands' energy was minimized before being translated to PDB format. The ligand was once more transformed into PDBQT format for the docking investigation by adding charges (Q) and bond types (T).

The specific amino acid residues implicated in this interaction were chosen from the string after the inhibitor, which bound to all of the receptors, was removed from the active site. Then, a suitable grid box that was sufficiently large to encompass all of the

interfering residues was generated. Utilizing the Lamarckian genetic algorithm, AutoDock version 1.5.6 was used to calculate the receptor-ligand interaction [51].

3.2.2 Molecular dynamic simulation

Molecular dynamics simulations were used to examine the docked complexes of 24 hydroxycholesterol-LXR-β, rifampicin-PXR, resveratrol-ASBT, and cilostazol-PDE in the Desmond module of the Schrödinger Maestro 2018.1 software. First, a simulation system comprised of a TI3P model and a cubic box built around the system of the docked complex was prepared using a system builder tool. Using a simulated annealing approach with 5000 iterations and a convergence limit of 1.0 kcal/mol, additional energy minimization of the constructed system was performed. The simulation run for the final 50 ns was completed, and the calculated trajectories were examined using the simulation interaction protocol [52].

3.2.3 Network pharmacology

3.2.3.1 Data formulation

From the GEO (http://www.ncbi.nlm.nih.gov/geo/) database, LXR and PXR gene expression profiles of GSE124053 (human hepatocytes) and GSE55746 (mouse hepatocytes) were downloaded [53-55]. Affymetrix GeneChip Human Gene 1.0 ST arrays were the basis for the microarray data for GSE124053, which includes 36 samples of primary human hepatocytes from two time periods, 4 h and 24 h (submission date: Dec. 18, 2018). In our investigation, we compared 24-hour cell culture data from the LXR agonist GW3965 with untreated control data. The GSE55746 data was similarly based on Affymetrix Mouse Genome 430 2.0 GeneChipsVR, and for our investigation, we examined the liver tissues of adult male wild-type mice treated with the PXR agonist pregnenolone-16-alpha-carbinonitrile (PCN) with control animals. (Date of submission: 10 Mar 2014).

3.2.3.2 Identification of differentially expressed genes (DEGs)

The DEGs were identified in the microarray dataset of hepatocytes (GSE124053, GSE55746) treated with LXR and PXR agonists using the GEO2R technique (https://www.ncbi.nlm.nih.gov/geo/geo2r/). Two criteria were used to filter out all DEGs: p-value 0.05 and $-1>\log_2 FC >+1$.

3.2.3.3 Pathway enrichment analysis

The ClueGo-v2.5.5 tool from Cytoscape was used for pathway enrichment analysis in order to find significant DEGs [56]. By using kappa statistics, which were adjusted at >0.4 in this study, we were able to construct and examine networks of functionally linked Gene Ontology (GO) terms.

3.2.3.4 Identification of hub-genes and sub-network analysis

Protein-protein interaction (PPI) networks were created using the STRING-v11.0 search engine and Cytoscape-v3.7.1 software. Modules of the PPI network was screened using the Molecular Complex Detection (MCODE-v1.6) approach from Cytoscape with degree cut-off = 2, node score cut-off = 0.2, κ-score = 2, and maximum-dept. = 100. The hub-genes were identified using the CytoHubba-v0.1 method. The top 10 nodes were highlighted as noteworthy hub-genes.

3.2.3.5 Ingenuity pathway analysis (IPA)

In order to analyze data and interpret molecular relationships within the context of canonical pathways and biological systems identified in the scientific literature and stored in the QKB (QIAGEN Knowledge Base), we used the IPA platform (QIAGEN, https://www.qiagenbioinformatics.com/products), a bioinformatics tool. Additionally, we have created customized pathways (i.e., visual connectivity maps) to display molecular networks using molecules connected to our model using a number of

IPA tools to test functional hypotheses (Figure 3). Between June 3rd and July 3rd, 2021, QKB provided the data that was used in this study.

3.2.3.6 IPA drug pathway procedure - identifying overlapping molecules

Using ‘My Pathway’ feature in IPA, drugs (rifampicin, resveratrol, metformin, cilostazol, 24- hydroxycholesterol) and receptors (LXR-β, PXR, PDE3B) were added to a new network. Then overlapping molecules between drugs and receptors were added to molecular network using the ‘Grow’ and ‘Pathway Explorer’ tools. Furthermore, ‘Connect’ tool was utilized to connect all molecules in the network without discriminating between directionality of relationship, so as to simulate how molecules and molecular networks in human body affect teach other and are rarely isolated. These molecular relationships added by ‘Grow’ and ‘Pathway Explorer’ tools were analyzed by using ‘Molecule Activity Predictor’ (MAP) tool. This tool predicts the activity of molecules, diseases, or Rifampicin, resveratrol, metformin, cilostazol, and 24-hydroxycholesterol were some of the medications and receptors that were added to a new network by using the IPA 'My Pathway' function. Other receptors were LXR-β, PXR, and PDE3B. Then, using the 'Grow' and 'Pathway Explorer' tools, overlapping molecules between drugs and receptors were added to the molecular network. In addition, the 'link' tool was used to link all of the molecules in the network without making any distinctions about the directionality of the relationships between them. This was done to imitate the way that molecules and molecular networks in the human body influence one another and are seldom seen in isolation. The 'Molecule Activity Predictor' (MAP) tool was used to investigate the molecular connections that were established by the 'Grow' and 'Pathway Explorer' tools, respectively. This tool simulates a change in the expression of a gene in order to anticipate the activity of molecules, diseases, or cellular functions when a molecule in a pathway has either been activated or deactivated. This allows the tool to predict the activity of molecules, diseases, or cellular functions. The

projected activity of the MAP tool was utilized, in conjunction with the literature results contained in the QKB pertaining to Alzheimer's disease, to analyze the association between medications and their activation of postulated receptors and their effects. In addition to that, this interpretation offered accurate quantitative insights that validated our proposed theory (Figure 3).

3.2.4 Synergy testing

Drug combinations were analyzed with SynergyFinder [57] using dose-response data for extracellular amyloid-beta levels with varying concentrations of rifampicin, resveratrol, cilostazol and metformin [48, 58-60]. Zero interaction potency (ZIP) and Bliss-models [61, 62] were chosen as the default parameter in SynergyFinder to calculate synergy scores (delta-score) for the interaction between the proposed drugs. Delta score was used to quantify deviation from expectation of zero interaction. A lower than zero delta implies a likely antagonistic interaction, while more than zero shows additivity or synergy between two tested drugs [63]. A similar score was generated for Bliss model, which assumes independent sites of action of two drug [61].

3.3 Results

3.3.1 Docking study

3.3.1.1 Molecular docking of amyloid beta

According to our theory, ABCG2 and ABCB1/MDR1 are involved in the transport of amyloid-beta. Although amyloid-beta cannot be docked into a binding site using conventional docking protocols because it is not a small molecule ligand, there are algorithms that can be used to predict protein-protein interactions. In order to establish the thermodynamic "best fit" for a particular protein pair, GRAMMX is a platform service that receives two proteins as inputs and runs a sizable number of unbiased simulations. We have employed the GRAMM-X technique in a similar way for other receptors such LXR-beta,

ASBT, and BSEP to demonstrate the binding affinity of amyloid beta with those receptors (Figure 4). Interacting residues were identified and displayed in Figure 5.

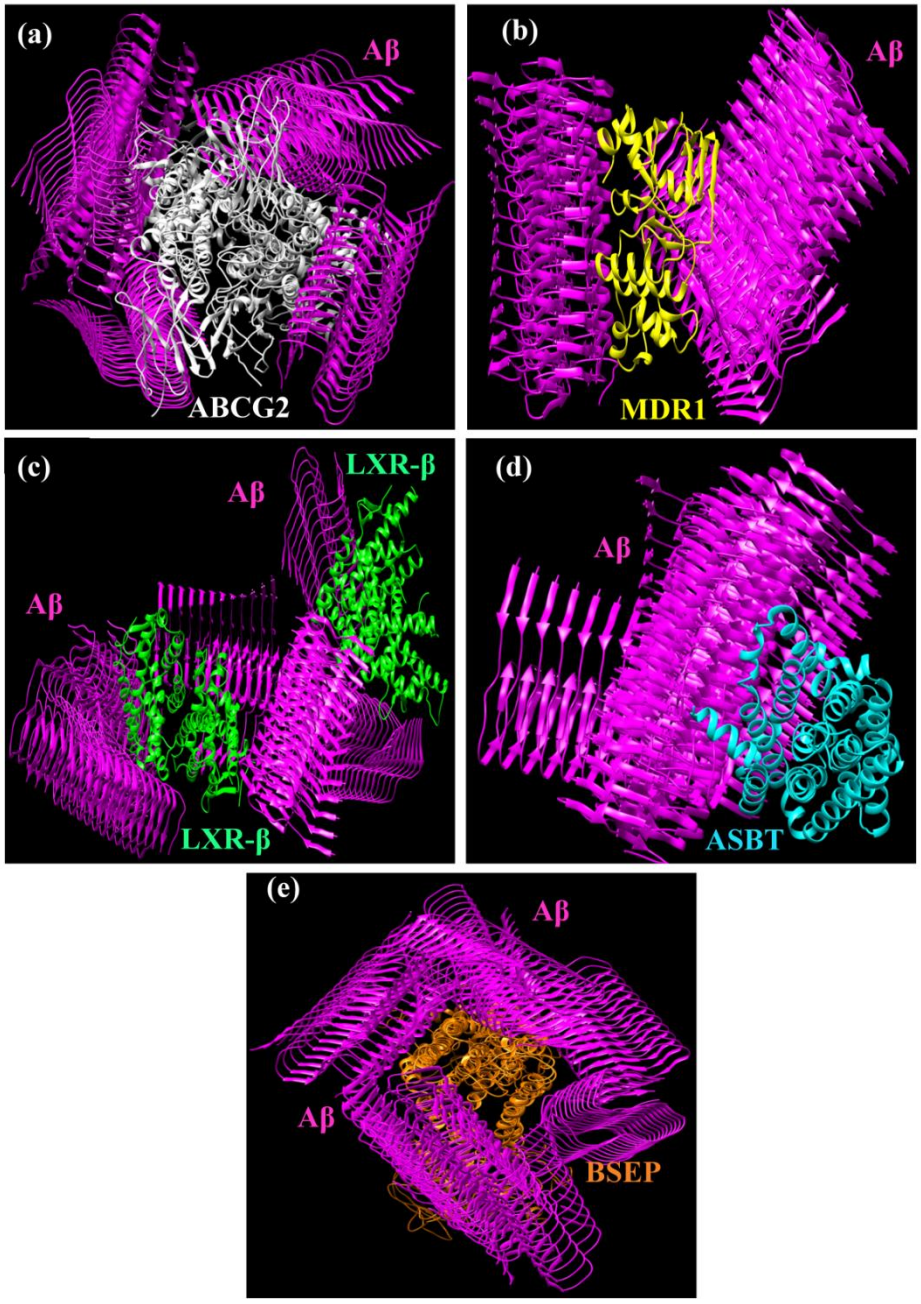

Figure 4: *Computed structural and binding features of the a) ATP-binding cassette super family G member 2 (ABCG2), b) Multidrug Resistance Protein 1 (MDR1), c)Liver X Receptor beta (LXR-beta), d) Apical sodium bile transporter (ASBT) and e) Bile salt export pump (e) with 42-residue human Aβ respectively. Human ABCG2 (PDBid: 6FEQ) in grey, MDR1 (PDB id: 2CBZ) in yellow, LXR-beta (PDB id: 1PQ6) in green, ASBT (PDB id: 3ZUX) in cyan, BSEP (PDB id: 6LR0) and Aβ (PDB id: 2 MXU) in pink color downloaded from PDB and used for the present study (Visualization using UCSF Chimera).*

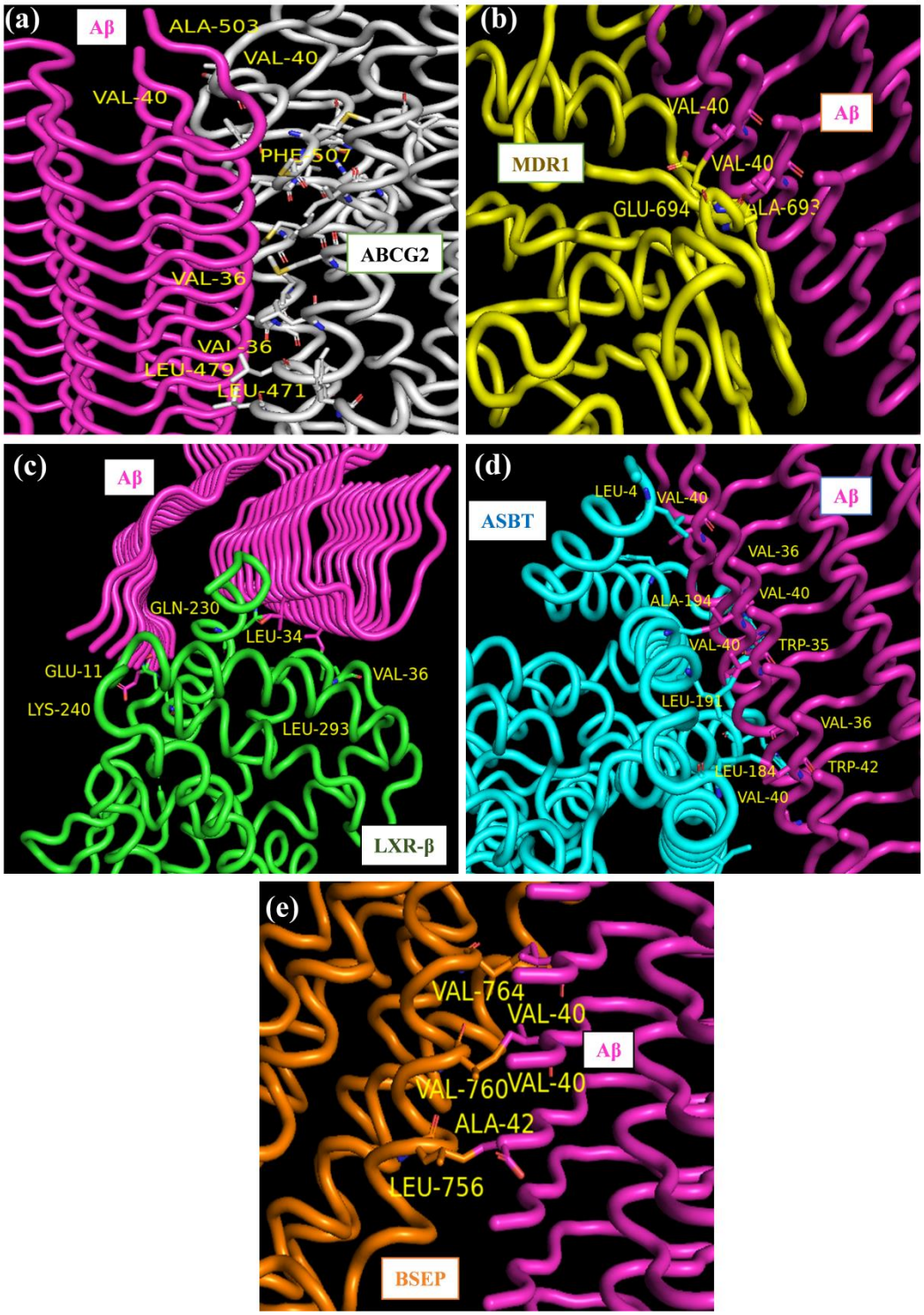

Figure 5: *Structural details at the interface between a) ABCG2, b) MDR1, c) LXR-beta, d) ASBT, e) BSEP and Aβ. Structural figures were made using PyMOL (the PyMOL Molecular Graphics System, v.2.0 Schrodinger).*

3.3.1.2 Molecular docking of repurposed drugs

Drug repositioning may be done relatively affordably by researching an existing drug for novel therapeutic uses. Rifampicin, cilostazol, metformin, and resveratrol are currently available medications for hypercholesterolemia, diabetes, vasoconstriction, and TB. As a result, we modified these drugs for AD and docked them with specific receptors where they acted as an agonist. Additionally, an LXR-β agonist known as 24-hydroxycholesterol has been reported to have an important role in cholesterol homeostasis and cardiovascular disease. Therefore, in the current investigation, we docked 24-hydroxycholesterol with the LXR-β receptor. The docking scores for rifampicin with PXR were -9.02 kcal/mol, for 24-hydroxycholesterol with LXR-β they were -10.75 kcal/mol, for resveratrol with ASBT they were -6.40 kcal/mol, for cilostazol they were -7.77 kcal/mol, and for metformin they were -4.30 kcal/mol (Figure 6). A comparatively low drug concentration is adequate to occupy a receptor and maximally elicit a physiological response. The binding energy is represented by the docking score, and the lowest binding energy indicates the maximum affinity of a drug towards a receptor. Additionally, Table 1 lists the crucial interacting amino acid residues.

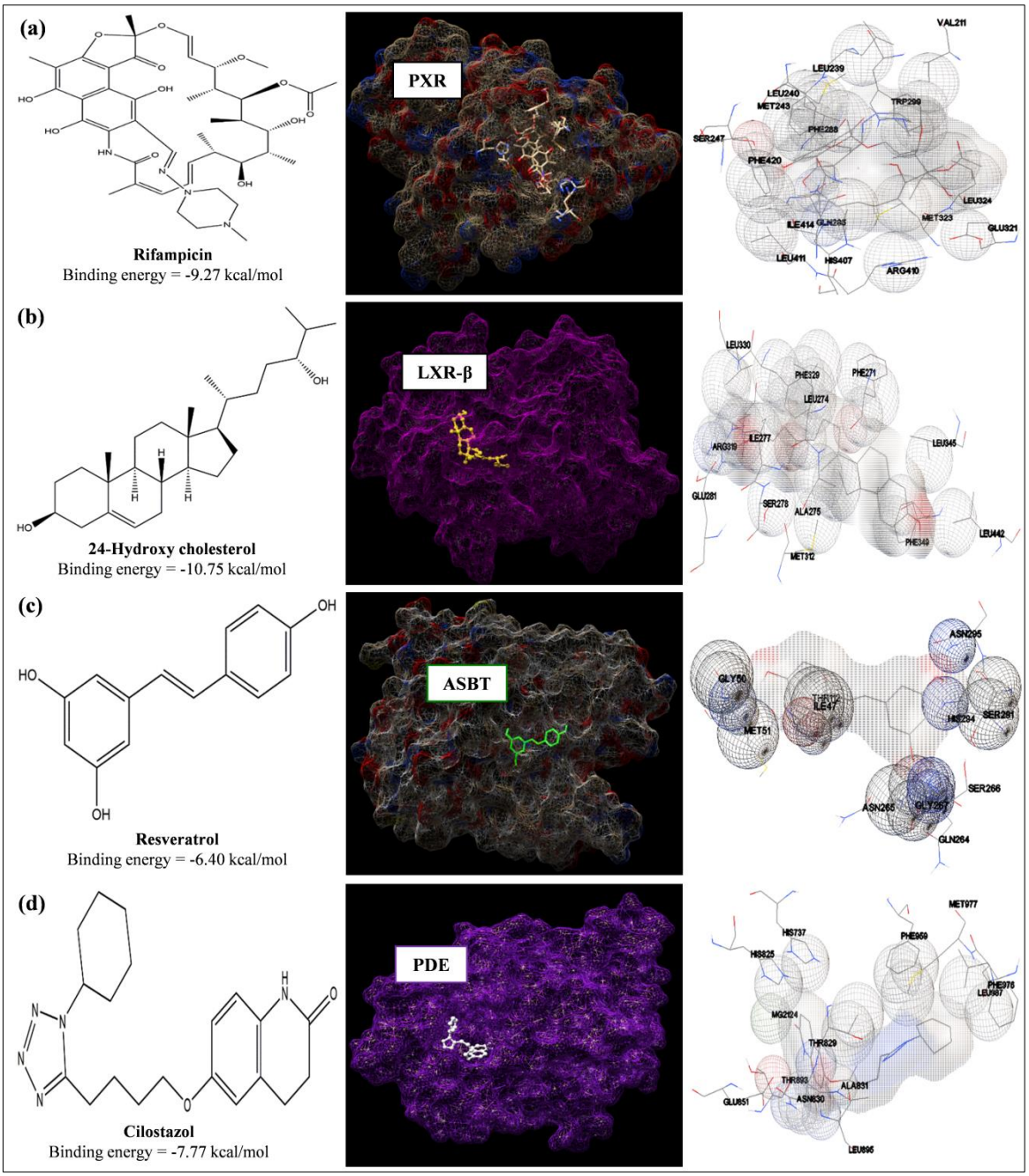

Figure 6: *Computed structural comparison and binding features (visualization using UCSF Chimera and AutoDock) of drugs rifampicin, 24-hydroxycholesterol, resveratrol, and cilostazol against PXR (PDB id: 1SKX), b) LXR-beta (PDB id: 1PQ6), c) ASBT (PDB id: 3ZUX), and d) Phosphodiesterase 3B (PDB id: 1SO2), respectively*

Table 1. The binding energy, inhibitory constant (Ki) value and interacting amino acid residues of drugs rifampicin, 24-hydroxycholesterol, resveratrol, cilostazol and metformin against PXR (PDB id: 1SKX), LXR-β (PDB id: 1PQ6), ASBT (PDB id: 3ZUX), Phosphodiesterase 3B (PDB id: 1SO2), and bile salt export pump (PDB id:6LR0) respectively.

Receptors	**Repurposed Drugs**	**Total binding energy (kcal/mol)**	**VDW + H bond + desolv Energy (kcal/mol)**	**Calculated inhibitory constant (Ki-Molar)**	**Interacting amino acid residues**
Pregnane X Receptor (PDB id: 1SKX)	Rifampicin	-9.02	-12.74	2.44×10^{-7}	Leu239 Leu240 Glu321 Phe420 His407 Gln285
Liver X Receptor-β (PDB id: 1PQ6)	24 Hydroxyl-cholesterol	-10.75	-12.73	1.31×10^{-8}	Ser278 Phe271 His435 Gln438 Phe329 Phe271
ASBT (PDB id: 3ZUX)	Resveratrol	-6.40	-7.73	2.03×10^{-7}	His294 Ser266 Thr112 Asn265 Gly267 Ser291
Phosphodiesterase 3B (PDB id: 1SO2)	Cilostazol	-7.77	-9.76	2.01×10^{-8}	His821 Asp822 Glu851 Phe959 Thr829 Ala831
Bile salt export pump (PDB id: 6LR0)	Metformin	-4.33	-1.56	6.67×10^{-8}	Thr355 Asp88 Ile91 Asp92 Val95 Gly357

3.3.2 Molecular simulation dynamics results

For docked complexes, solvent accessible surface area (SASA), molecular surface area (MolSA), and polar surface area (PSA) parameters were calculated using MD simulation and other parameters, including root mean square deviation (RMSD), root mean square fluctuation (RMSF), protein-ligand contact time, radius of gyration (Rg), and solvent accessible surface area (SASA).

3.3.2.1 Root mean square deviation

The RMSD calculates the average displacement shift of a set of atoms for a given frame relative to a reference frame. The RMSD value of the simulated trajectory for the rifampicin-PXR complex was measured at a maximum of 2.4 and remained constant throughout the whole 50 ns period (Figure 7a). A maximum value of 2.7 RMSD was observed for the 24 hydroxycholesterol-LXR-beta combination, which also demonstrated consistent stability (Figure 8a). The RMSD value for the resveratrol-ASBT combination dropped until 12 ns, then steadily increased and remained steady for the remaining duration (Figure 9a). The RMSD value for the cilostazol-PDE combination remained consistent over the course of the experiment and was within the acceptable range (Figure 10a).

3.3.2.2 Root mean square fluctuation

RMSF allows for the detection of local alterations throughout the protein chain. These values were estimated utilizing the enzymes' Ca atoms to get insight into the structural variations of active amino acid residues caused by ligands [64]. The RMSF graph for the rifampicin-PXR complex remained constant throughout the simulation, and protein residues that interact with the ligand are shown by green vertical bars (Figure 7b). The RMSF graph for the other complexes was similarly steady with mild oscillations (Figure 8b, Figure 9b, Figure 10b).

3.3.2.3 The radius of gyration (Rg) and solvent accessible surface area (SASA)

Each complex's compactness is measured by the Rg. Rg values for rifampicin-PXR, 24-hydroxycholesterol-LXR-β, and 5.7, respectively. According to the figure, all of the complexes had comparable stability patterns throughout the experiment. Furthermore, using MD simulation, the SASA calculated the surface area of the ligand accessible to the solvent. The cilostazol-PDE combination had a larger average SASA (200) than the other complexes (Figure 7c, as well as Figure 8c, Figure 9c, and Figure 10c).

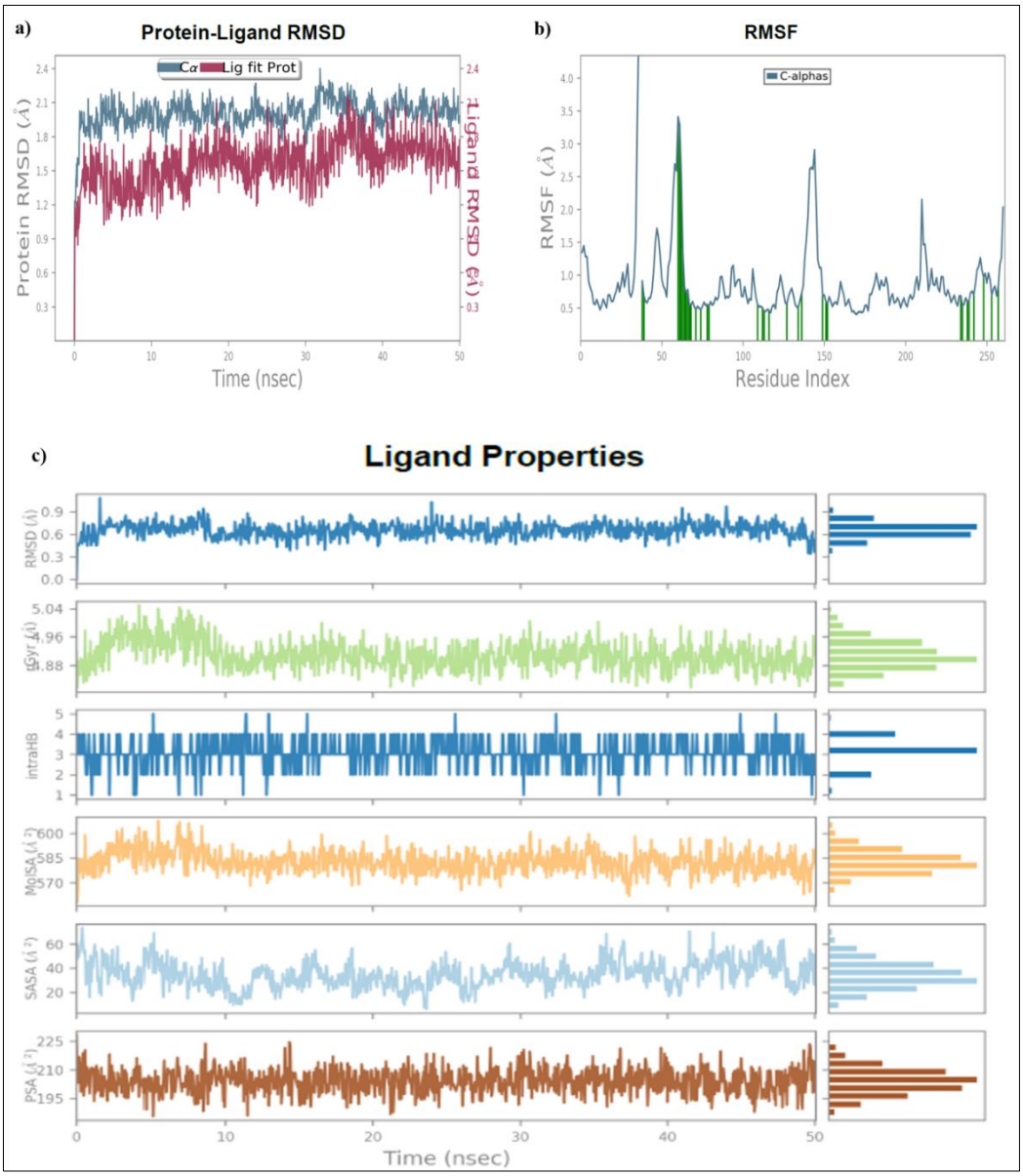

Figure 7: *(a) The root mean square deviation (RMSD); (b) The root mean square fluctuation (RMSF); and (c) graphs of ligand properties for the rifampicin during50 ns simulation runs on PXR (pregnane X receptor).*

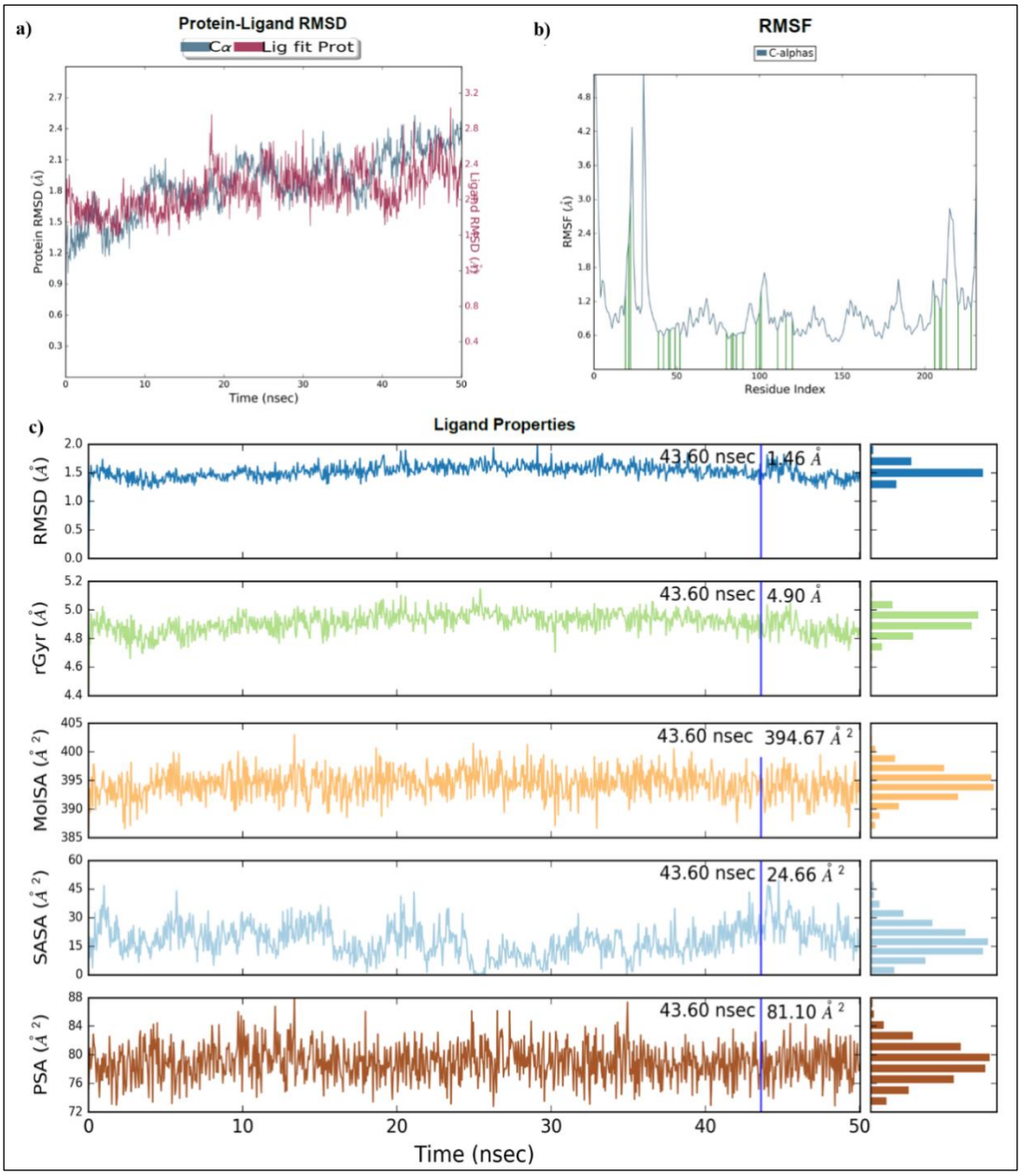

Figure 8: *(a) The root mean square deviation (RMSD); (b) The root mean square fluctuation (RMSF); and (c) Ligand properties graph for the 24-hydroxycholesterol during 50 ns simulation runs on LXR-β (liver X receptor).*

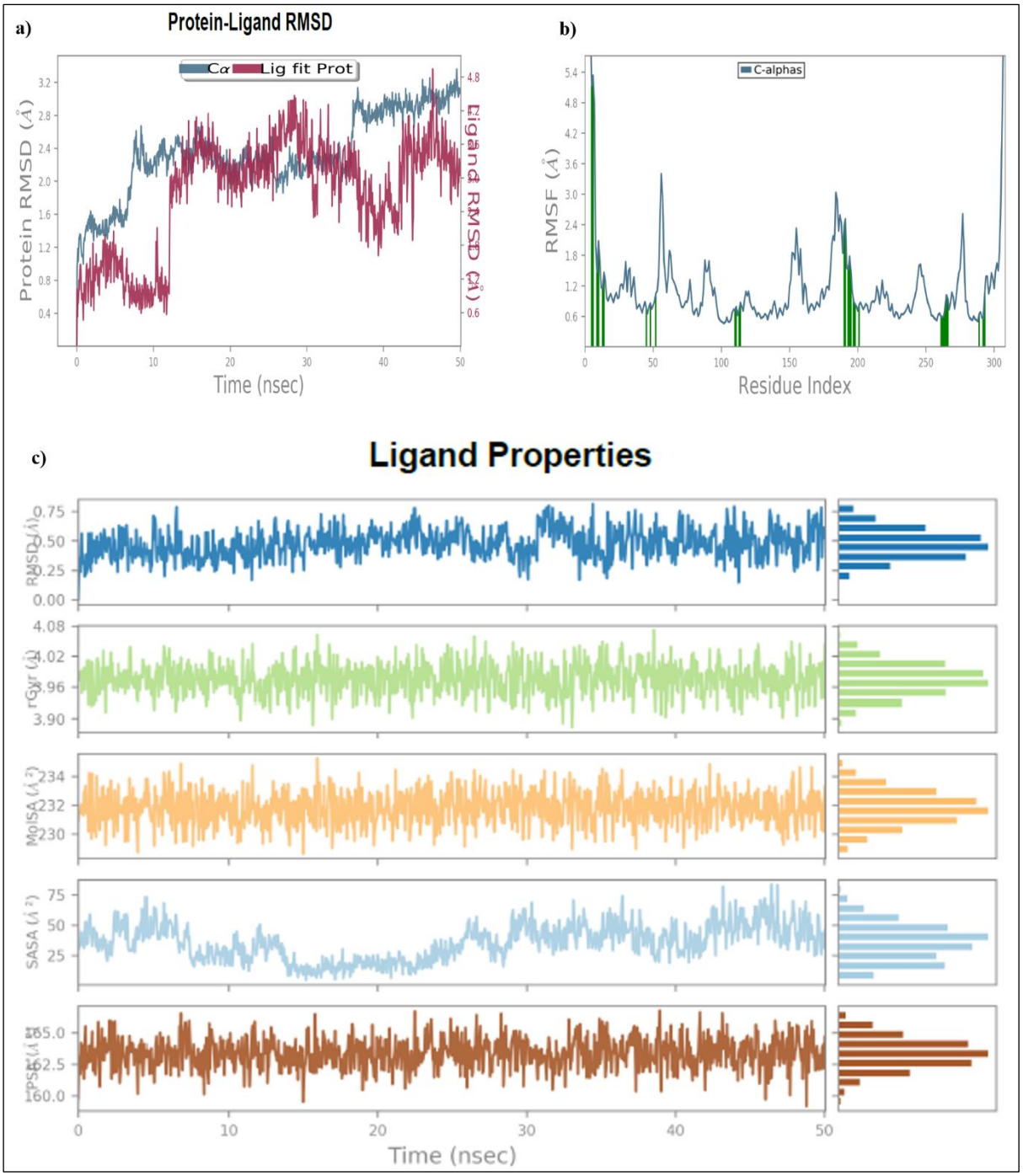

Figure 9: *(a) The root mean square deviation (RMSD); (b) The root mean square fluctuation (RMSF); and (c) Ligand properties graph for the resveratrol during 50 ns simulation runs on ASBT (Apical Sodium-Dependent Bile Acid Transporter).*

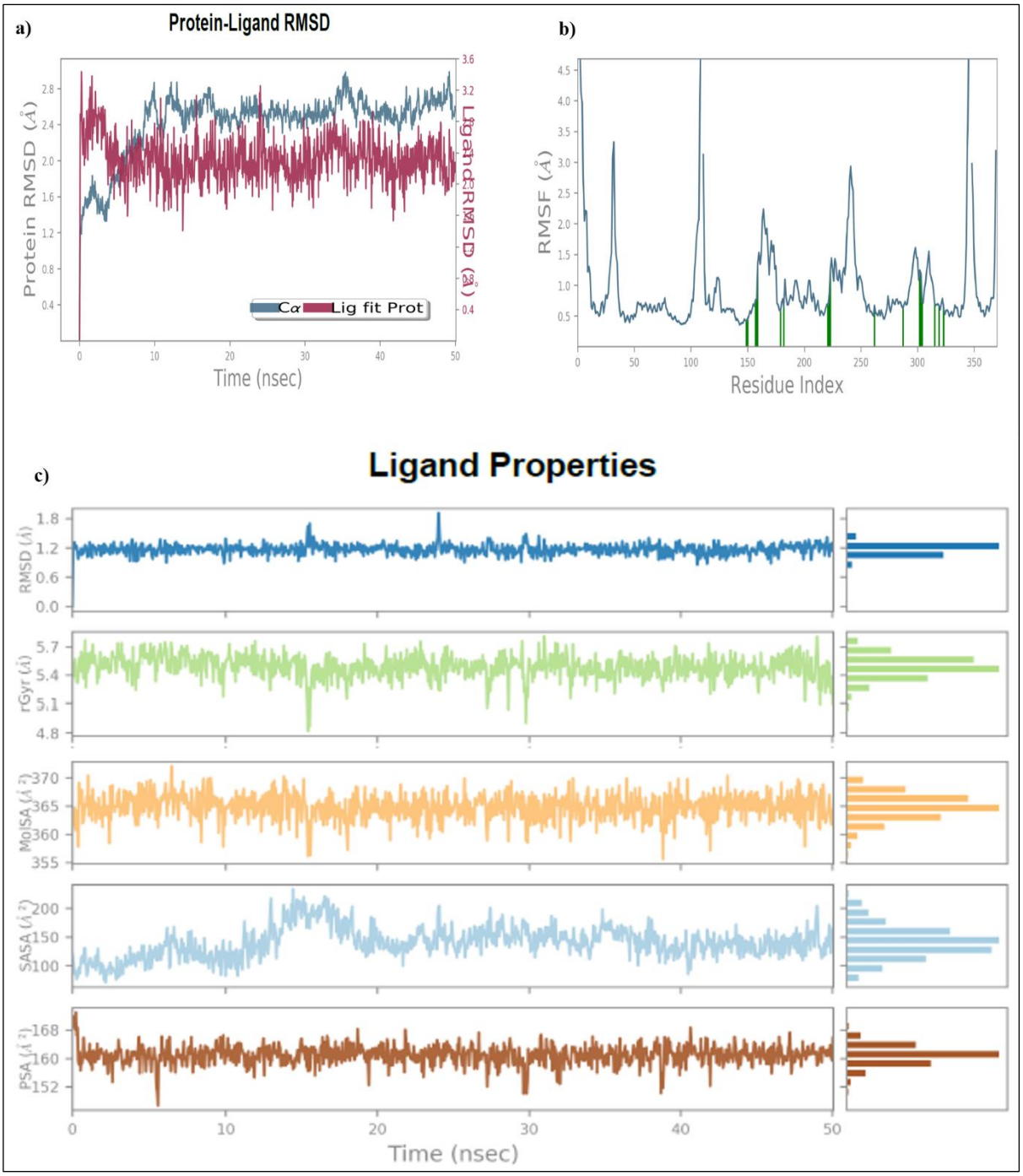

Figure 10: *(a) The root means square deviation (RMSD); (b) The root mean square fluctuation (RMSF); and (c) Ligand properties graph for the cilostazol during 50 ns simulation runs on PDE3 (Phosphodiesterase-3).*

3.3.2.4 Protein-ligand contact

Interaction percentages were shown using stacked bar charts in the interaction analysis for all complexes. The graphical depiction displayed interactions, delimited percentage interactions, and interacting residues on the timeline. Rifampicin interaction studies on PXR revealed a strong hydrogen bond with Gln285 and His407 residues. Furthermore, during simulation contact, water bridge formation was seen with Leu239 and Glu321 residues (Figure 11). Similarly, 24-hydroxycholesterol connected with Ser278, His435, and Gln438 residues in LXR-β, producing a hydrogen bond. Furthermore, several notable hydrophobic interactions with Phe271 and Trp457 were found (Figure 12). The examination of resveratrol interactions with ASBT indicated significant hydrogen bonding with Ser291, His294, and Gly267 residues, as well as water bridge formation with Thr54 residue (Figure 13). Furthermore, cilostazol interaction study on PDE3 revealed ionic contact via magnesium ions. To put this in context, it should be noted that secondary research indicates that seven of the PDE subfamilies require such divalent metal cations for catalytic activity [88]. Cilostazol interacted with Mg^{2+} through Asp822, His821, and Glu851 residues, according to our modeling results. Cilostazol also built a water bridge with Asn830 residue and produced a hydrophobic interaction with Phe959 (Figure 14).

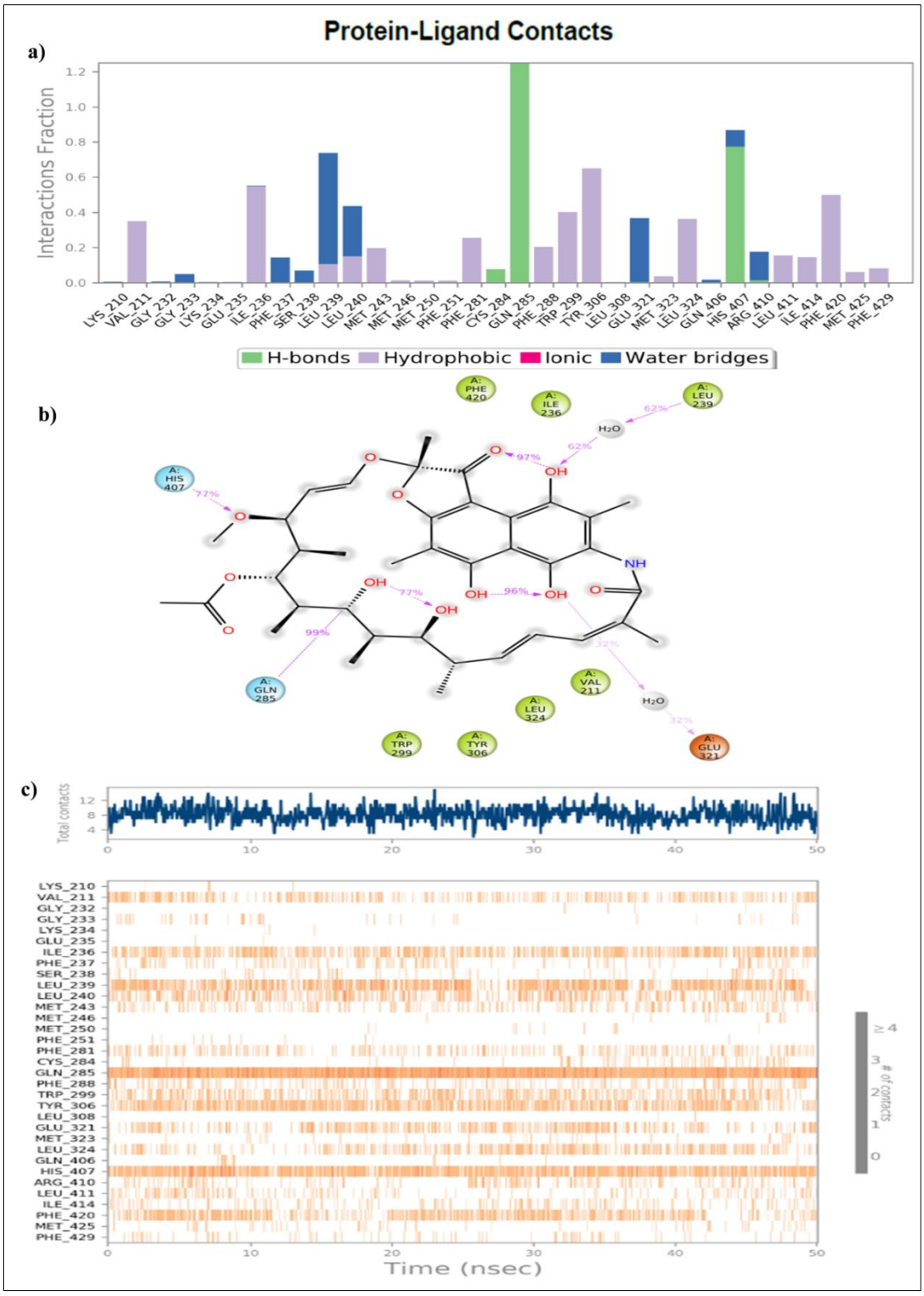

Figure 11: *(a) Stacked bar chart representation of rifampicin with active site amino acid residues of PXR (pregnane X receptor); (b) Ligand-protein contacts of rifampicin-PXR complex, and (c) Timeline representation for 50 ns simulation run analysis of rifampicin and PXR docked complex.*

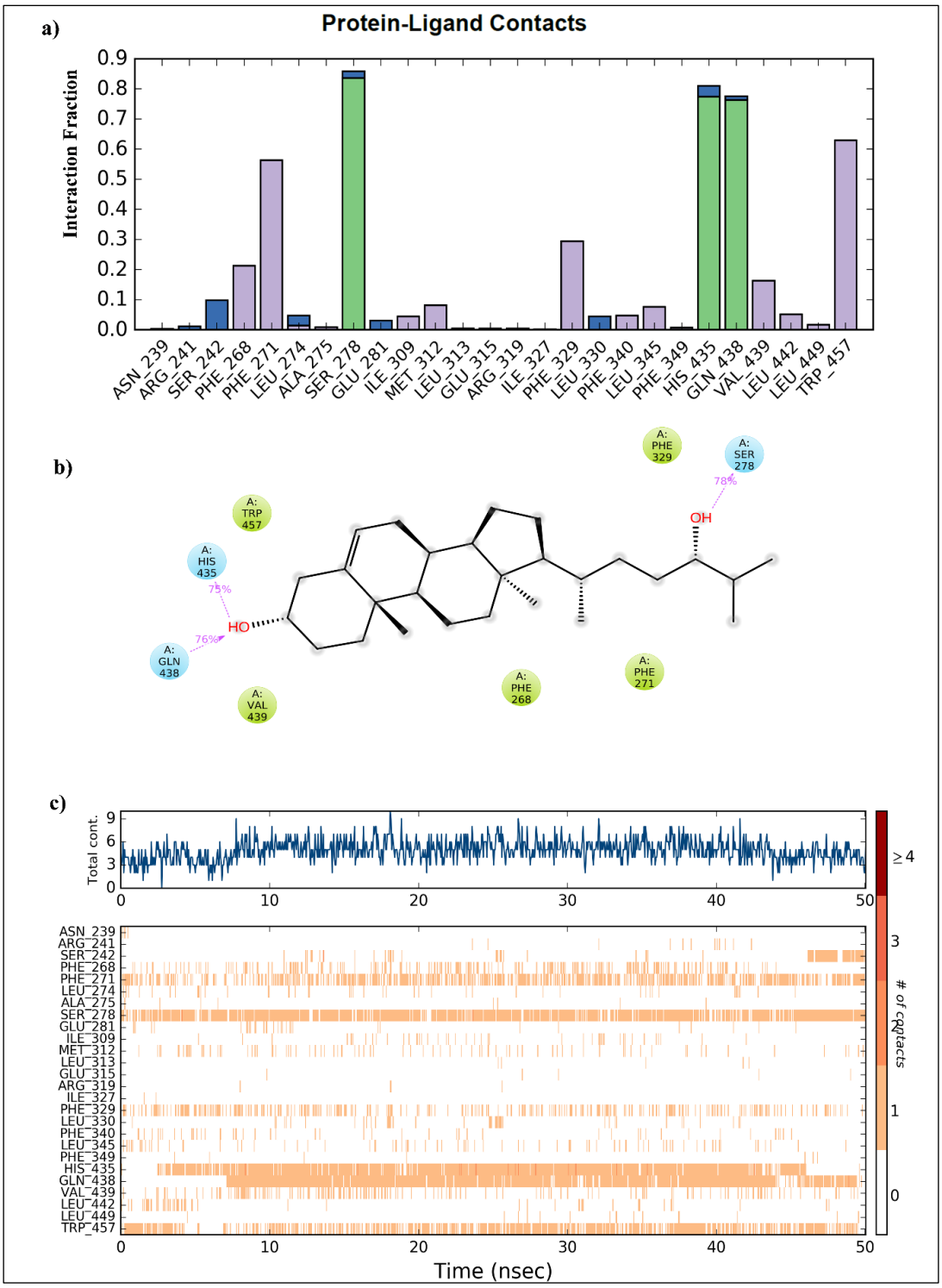

Figure 12: *a) Stacked bar chart representation of 24-hydroxycholesterol with active site amino acid residues of LXR-β (liver X receptor); b) ligand-protein contacts of 24-hydroxycholesterol-LXR-β complex and c) timeline representation for 50 ns simulation run analysis of 24-hydroxycholesterol and LXR-β docked complex.*

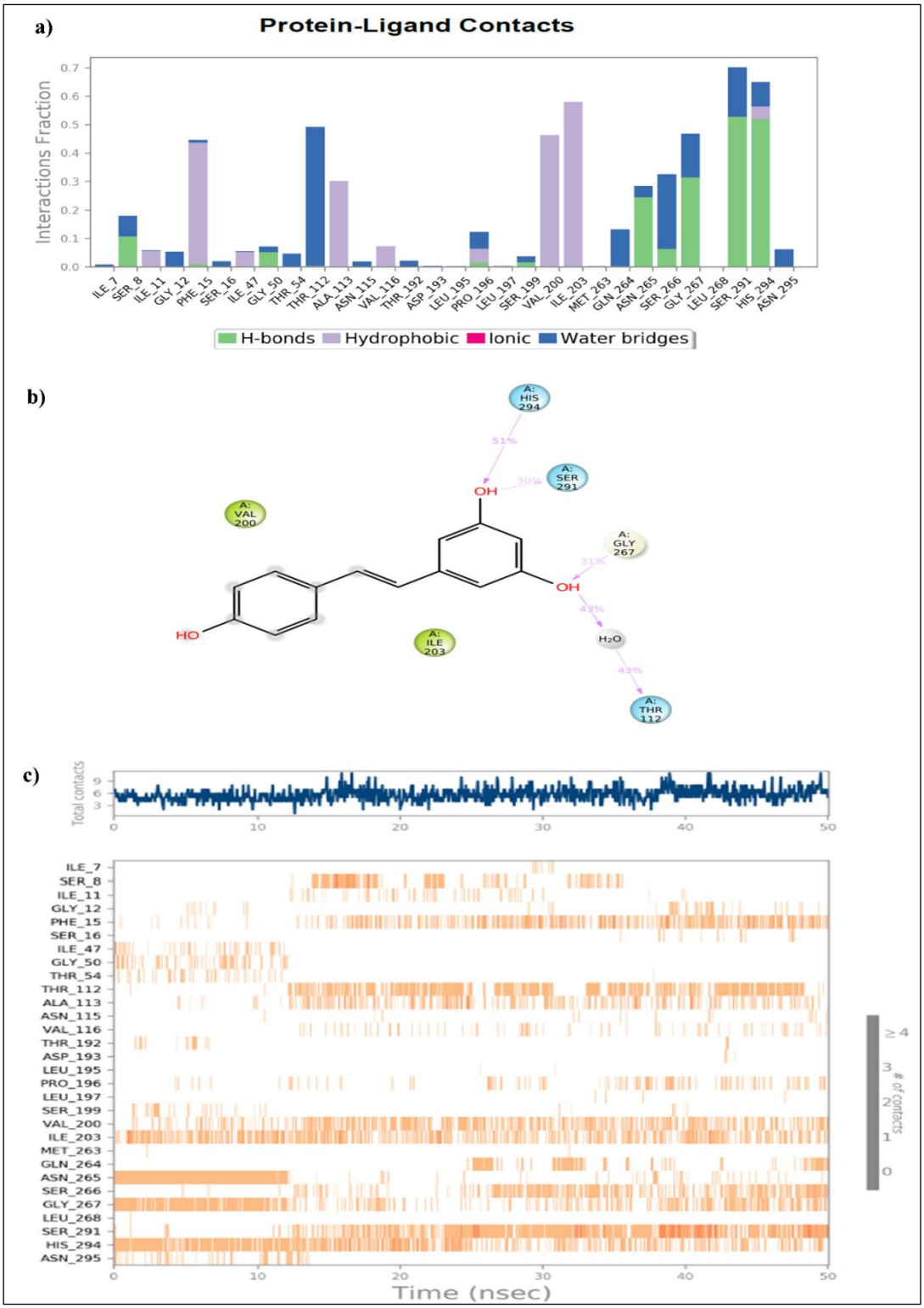

Figure 13: *a) Stacked bar chart representation of resveratrol with active site amino acid residues of ASBT (Apical Sodium-Dependent Bile Acid Transporter); b) ligand-protein contacts of resveratrol-ASBT complex and c) timeline representation for 50 ns simulation run analysis of resveratrol and ASBT docked complex.*

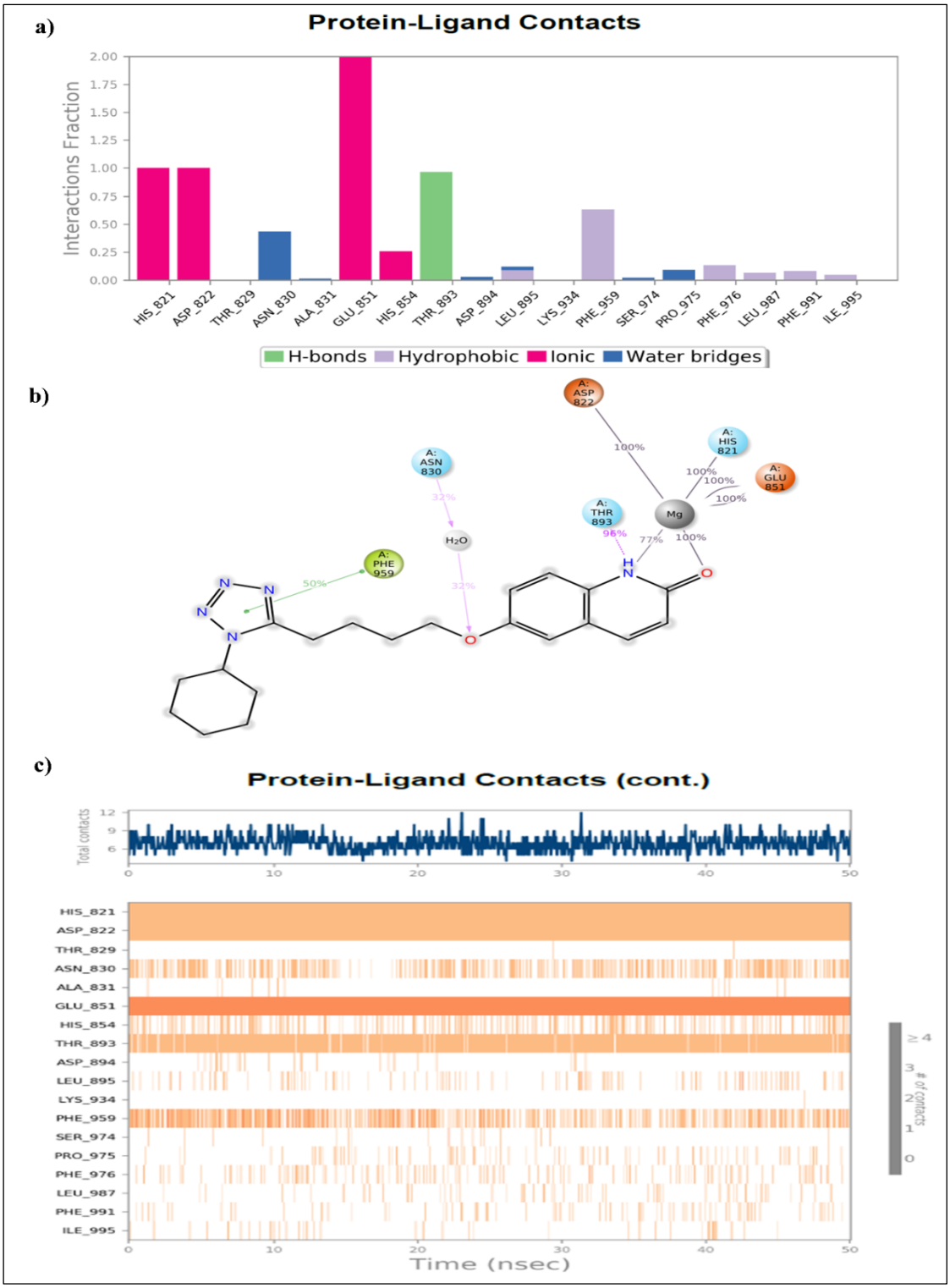

Figure 14: *a) Stacked bar chart representation of cilostazol with active site amino acid residues of PDE3 (Phosphodiesterase-3); b) ligand-protein contacts of cilostazol -PDE3 complex and c) timeline representation for 50 ns simulation run analysis of cilostazol and PDE3 docked complex.*

3.3.3 Network pharmacology analysis

3.3.3.1 Identification of differentially expressed genes (DEG)

This analysis includes two gene expression profiles of liver tissues, GSE124053 and GSE55746 [77, 78]. Genes having a 2-fold change in expression value and a p-value less than 0.05 were filtered. From the expression profile datasets GSE124053 and GSE55746, we retrieved 722 and 534 DEGs, respectively. The GSE datasets identified differentially expressed genes were divided into two groups: upregulated and downregulated genes. The criteria listed above discovered 17 upregulated genes in the GSE124053 dataset and 411 upregulated genes in the GSE55746 dataset. LXR activation increases the amount of ABCA1 and SCD expression, while PXR activation increases the level of ABCB1 expression (Figure 15).

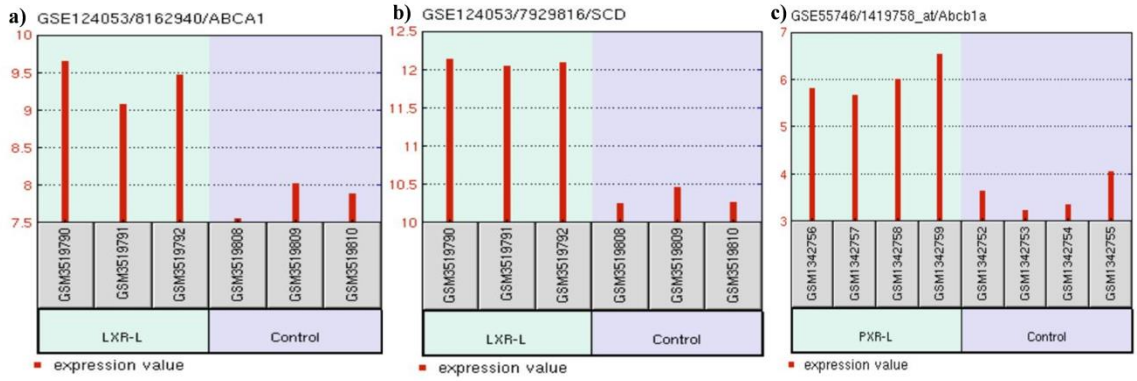

Figure 15: *The GEO2R analysis showed that LXR agonist and PXR agonist upregulates expression of a) ABCA1, b) SCD, and c) ABCB1 genes.*

3.3.3.2 Gene ontology analysis

The Cytoscape ClueGO technique was used for gene ontology analysis, which allowed for functional investigation of DEGs. Using the STRING-database, the PPIs of DEGs were built (Figure 16a, b). CluGO analysis revealed that the GSE124053 gene expression profile upregulated genes involved in the sterol metabolic process (green nodes) (Figure 17a), while the GSE55746 dataset upregulated genes involved in the detoxification (pink nodes), cell cycle regulation (brown nodes), and collagen regulation (blue nodes) (Figure 17b). Using Cytoscape's CytoHubba platform, we then ranked the genes with the most hub nodes in the PPI network. Figure 18a shows that ABCA1 and SCD are among the most elevated genes in relation to cholesterol efflux, and Figure 18b shows that genes linked to cell-cycle modulators are increased in the GSE55746 dataset. Genes involved in cholesterol efflux, such as ABCA1 and SCD, have been shown to play a role in lowering amyloid beta production. After that, MCODE was used to conduct a sub-network analysis (Figure 19). Consequently, among the elevated genes in (i) the GSE124053 profile of LXR-β and (ii) the GSE55746 profile of PXR (Table 2), the ACSS2 and Mcm6 genes appeared as seed nodes, respectively.

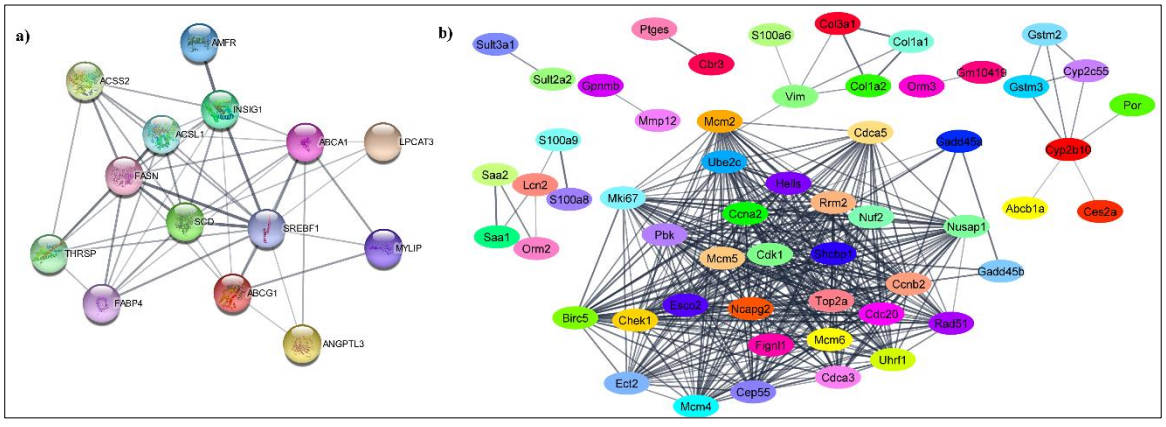

Figure 16: *Protein-protein interaction networks (PPIs) of DEGs were constructed using STRING database, upregulated genes for a) GSE124053 profile of LXR-β, and b) GSE55746 profile of PXR*

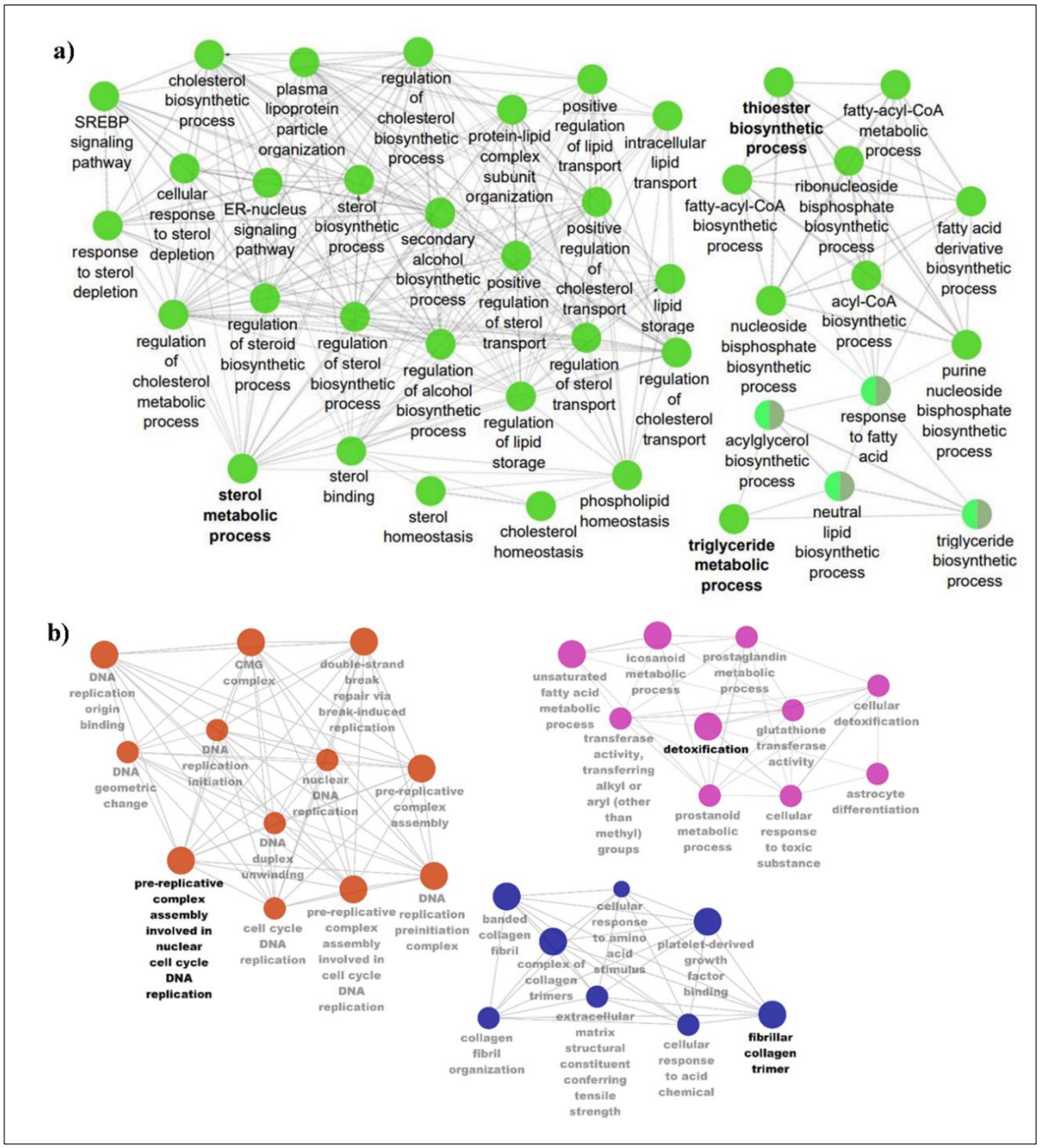

Figure 17: *Gene ontology analysis was performed for functional analysis of DEGs by using ClueGo app from Cytoscape. This app allows simultaneous analysis of multiple annotation and ontology sources. Functionally grouped network is represented, a) upregulated genes for GSE124053 dataset and b) upregulated genes for GSE55746 dataset. The node size represents enrichment significance and connections are based on kappa score (> 0.4). In upregulated gene group forGSE124053 profile shows maximum number of nodes which are in green color represent the sterol and triglyceride metabolic process and GSE55746 profile showscell cycle process (brown nodes), detoxification (pink nodes) and collagen related (blue nodes)*

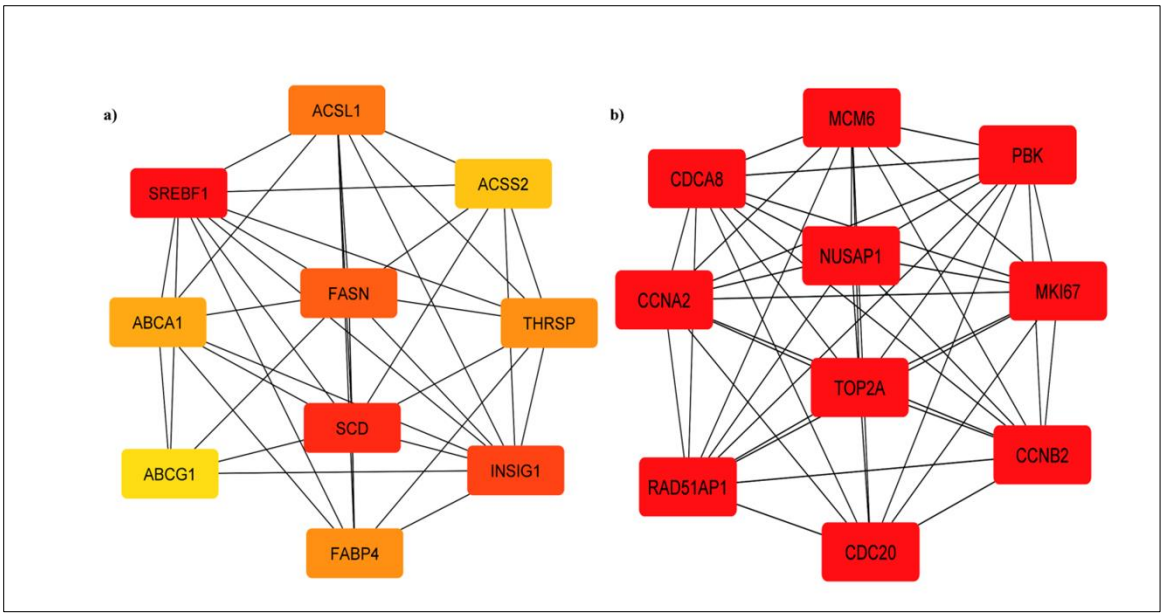

Figure 18: *Genes with the greatest changes in expression. We observed that the top ranked hub genes in PPI network which were upregulated were associated with a) cholesterol efflux and b) cell cycle regulator.*

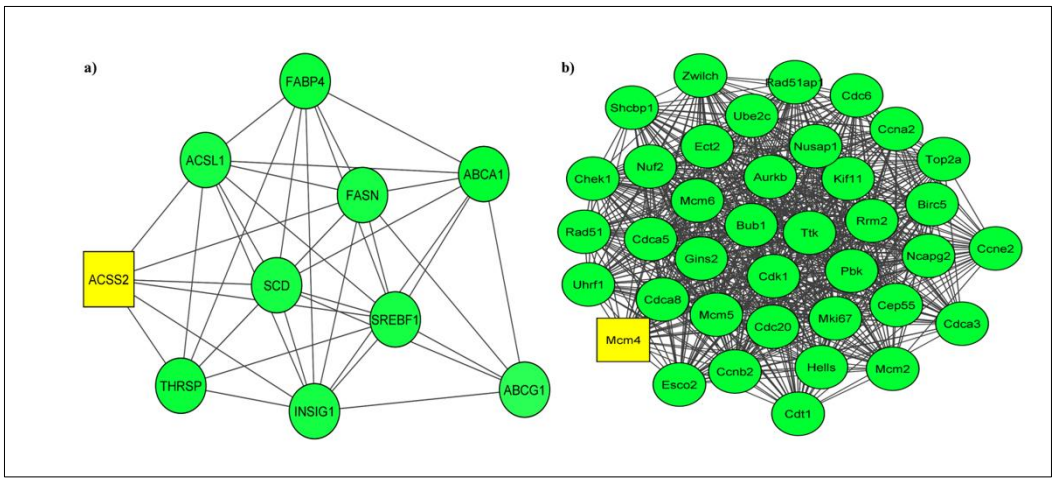

Figure 19: *Sub-network analysis was conducted by using the Molecular Complex Detection (MCODE) app from Cytoscape. Top sub-networks on the basis of MCODE score (Degree cut-off = 2, node score cut-off = 0.2, k-core = 2 and max. depth = 100). Upregulated gene group clusters, we identified seed nodes (ACSS2 and Mcm6) for GSE124053 profile of LXR and GSE55746 profile of PXR (highlighted in yellow) respectively.*

Table 2. Functions of top ranked hub genes.

Rank	GSE124053 Up regulated genes	UniportKB/Swiss-Prot Function	GSE55746 Up regulated genes	UniportKB/Swiss-Prot Function
1	SREBF1	Regulates transcription of the LDL receptor gene as well as the fatty acid	Ccnb2	Essential for the control of the cell cycle at the G2/M (mitosis) transition
2	SCD	Stearoyl-CoA desaturase plays an important role in lipid biosynthesis	Cdc20	Cell division cycle protein
3	INSIG1	Insulin-induced gene 1 protein mediates feedback control of cholesterol synthesis	Ccna2	Cyclin which controls both the G1/S and the G2/M transition phases of the cell cycle
4	FASN	Fatty acid synthetase catalyzes the formation of long- chain fatty acids from acetyl-CoA, malonyl-CoA and NADPH	Mki67	Required to maintain individual mitotic chromosomes dispersed in the cytoplasm following nuclear envelope disassembly
5	ACSL1	Activation of long-chain fatty acids for both synthesis of cellular lipids, and degradation via beta-oxidation	Top2a	Control of topological states of DNA by transient breakage and subsequent rejoining of DNA strands
6	FABP4	Lipid transport protein in adipocytes	Nusap1	Microtubule-associated protein with the capacity to bundle and stabilize microtubules
7	THRSP	Plays a role in the regulation of lipogenesis	Rad51ap1	Participate in a common DNA damage response pathway associated with the activation of homologous recombination and double-strand break repair
8	ABCA1	Key gatekeeper influencing intracellular cholesterol transport	Cdca8	Component of the chromosomal passenger complex (CPC), a complex that acts as a key regulator of mitosis
9	ACSS2	Activates acetate so that it can be used for lipid synthesis or for energy generation	Pbk	Lymphokine-activated killer T-cell-originated protein kinase
10	ABCG1	Transporter involved in macrophage lipid homeostasis	Mcm6	Minichromosome maintenance complex component helps in DNA replication initiation and elongation in eukaryotic cells

3.3.3.3 Interconnected pathway analysis of proposed drugs and receptors

The molecules related to proposed drugs and receptors were identified using IPA's 'My Pathway' feature and build tools. The proposed drugs and receptors were linked, and their biological activity was predicted using IPA's MAP tool. Based on color saturation, the MAP tool may visually measure the projected action of suggested drugs on receptors: orange signifies excitation (upregulation), while blue represents inhibition (downregulation). Colors that are more saturated suggest a larger amount of change. As a result, we can observe that the drug molecule cilostazol inhibits PDE-3 and activates the cAMP (cyclic Adenosine Monophosphate) pathway, while raising the expression of ABCA1 and SCD genes (orange hue), which are likewise elevated by LXR activation. Similarly, rifampicin stimulates the NR1I2/PXR receptor, which increases ABCB1/MDR1 gene expression (orange), but resveratrol decreases ASBT/SLC10A2 gene expression (blue) (Figure 20), supporting our theory.

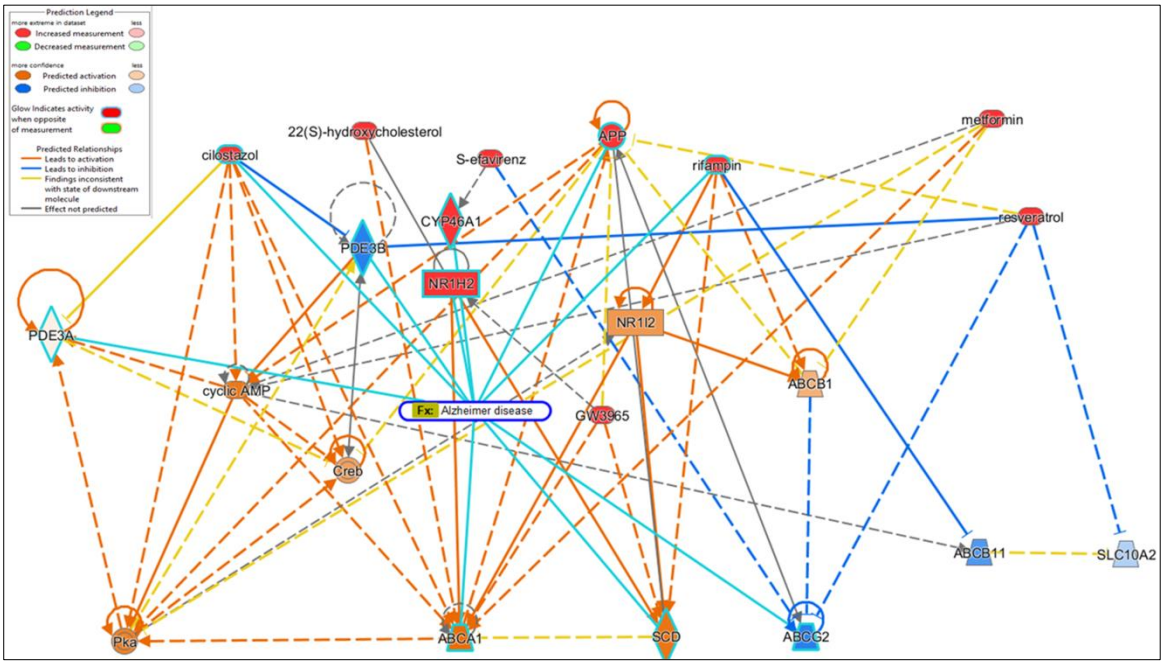

Figure 20: *Connectivity Map of the relationships of the drug molecules with receptors, and intermediary molecules are interconnected between themselves to simulate reciprocal relationships (upstream and downstream).*

3.3.4 Validation Analysis for clinical efficacy

In this section, we outline the clinical validation of our proposed drugs (metformin, rifampin, resveratrol, and cilostazol) for AD. Table 3 provides details on the parameters. Regarding the numerous human trials conducted, the patient populations range from n = 40 to 120, and the drugs were administered separately (not in combination). All of the studies are statistically significant, with some clinical trials having p-values as low as 0.002. We delineate that the findings are robustly indicative that there should be further escalation, on priority basis, to multi-centric clinical trials of Phase 3 and Phase 4 stages.

Table 3. Clinical trial data for individual proposed repurposed drugs.

Proposed Drugs	Presume mechanical pathway	Dose/Dose regimen	Preclinical/Clinical Investigation	Outcome
Rifampicin	Targeting AD-type hypo- metabolism	450 mg/d for 1 Year	Enrolled 40 non-demented elderly patients having mycobacterium infections and AD-type hypo-metabolism	The metabolic change in the posterior cingulate cortex between therapy for 12 and 6 months was significantly different in repeated measures ANCOVA ($p = 0.009$) [65]
Resveratrol	Decreasing MMP9 level in CSF, modulating neuroinflammation, and inducing adaptive immunity	500 mg/d with dose escalation by 500-mg increments every 13 weeks, ending with 1,000 mg twice daily	Randomized, placebo-controlled, double-blind, multicenter 52-week phase 2 trial in 119 adults with mild to moderate Alzheimer disease	Reduce level of CSF ($p = 0.002$) and plasma ($p = 0.024$) beta-amyloid[66, 67]
Metformin	Decreases amyloid load causing increase in pulsatality of orbito-frontal cerebral blood flow	500 mg per week until a maximum of 2000 mg/dfor 8 weeks	Randomized, placebo-controlled, 8-week in 20 nondiabetic subjects with mild dementia due to AD	Statistical trend in improving learning and memory ($p = 0.06$) [68]
Cilostazol	Increases glucose metabolism	100 mg (50 mg twice daily) increased to 200 mg (100 mg twice daily) after 2 weeks	Randomized, double-blind, placebo-controlled, parallel-group single-center 24-week study in AD patients	Significant increase in cerebral glucose metabolism ($p < 0.005$) improving or protecting cognitive function in Alzheimer's disease[69]

3.3.5 Combination therapy

Multiple pathophysiologies can be targeted by drug combinations, which explains the efficacy of combination treatments for Alzheimer's disease. In comparison to a single drug, a combination of drugs performs well when the synergistic effects of the drugs generate greater therapeutic efficacy than the individual therapeutic agent. According to the ZIP and BLISS synergy scores, the combination of rifampicin, cilostazol, and metformin was more synergistic than other combinations (Figure 21). In addition, the contour plot of SynergyFinder Plus (Figure 22) revealed that the combination of rifampicin and metformin had the highest synergy score.

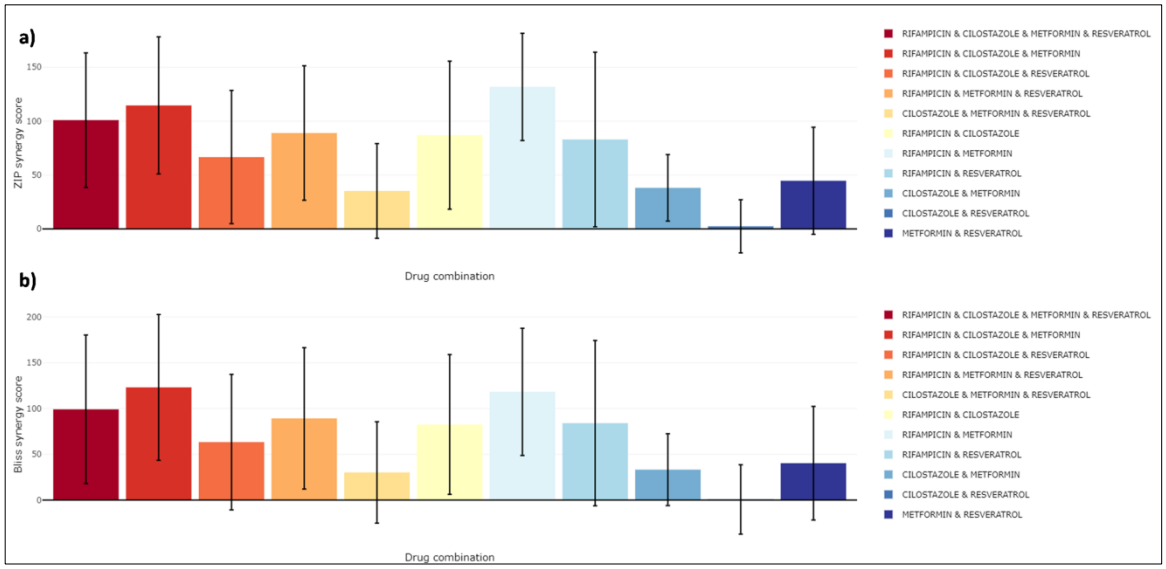

Figure 21: *Synergy score a) Zero Interaction Potency (ZIP) and b) Bliss for drug combinations.*

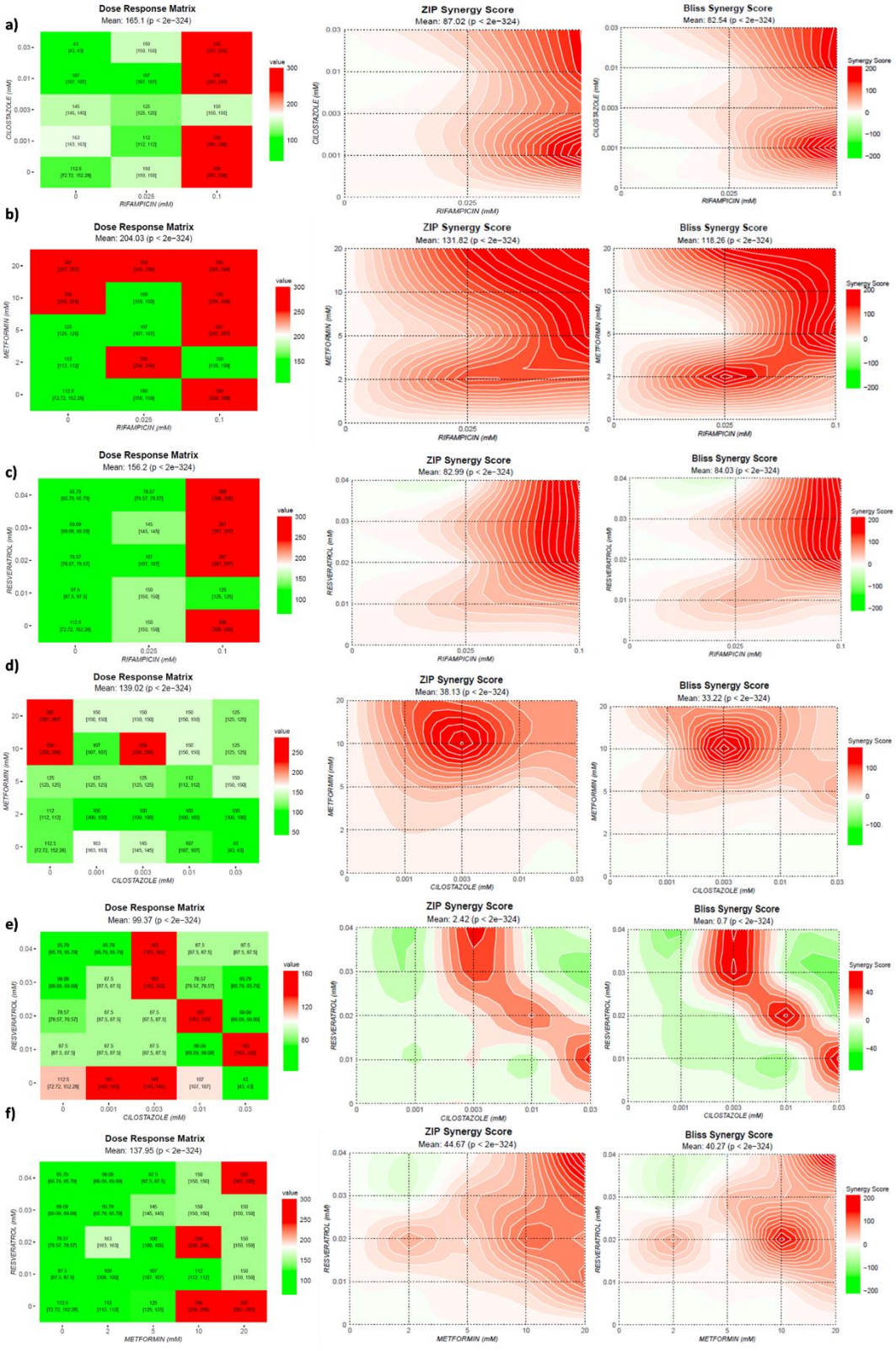

Figure 22: *From left to right, dose-response, ZIP, Bliss synergy metrics in contour plot format were generated using the SynergyFinder web tool. The darker redcolor represents high synergy for each drug concentration in the combination. Synergy is presented for a combination of cilostazol with rifampicin (a), metformin with rifampicin (highest synergy) (b), resveratrol with rifampicin (c), metformin with cilostazol (d), resveratrol with cilostazol (e), and resveratrol with metformin (f). Data are represented as the mean of samples.*

3.4 Discussion

In the current work, we have demonstrated for the first time that amyloid beta undergoes the entero-hepatic circulation (EHC) process. Pharmacological modification of the EHC process might be an AD treatment strategy based on our systems analysis. An imbalance between amyloid-beta synthesis and clearance causes an increase in amyloid beta burden in the brain. An interventional measure can be a drug that increases the organism's ability to excrete or eliminate amyloid-beta (through bile and feces).

It has been suggested in a number of studies that the liver is the major organ that has the largest concentration of amyloid-beta [70]. In addition, the liver is the organ responsible for the most significant amount of peripheral clearance of plasma amyloid-beta [71]. Furthermore, Mohamed et al. revealed that amyloid-beta undergo biliary clearance in their in-vitro examination with primary rat hepatocytes, which indicates that amyloid-beta is transported via the EHC [12].

ASBT is one of the receptors that we have identified as being responsible for the reabsorption of amyloid-beta from the liver back into the systemic circulation and brain via EHC. In addition, we have identified several genes, such as ABCG2, ABCB1/MDR1, and ABCB11 gene encoded BSEP, whose higher expression can promote more amyloid-beta efflux and elimination. These genes include ABCB11 gene encoded BSEP. Additionally, the genes known as ABCA1 and SCD are essential to the process of lowering the production of amyloid-beta. Since our protein-protein docking data demonstrated that amyloid-beta interacts with ASBT, which is important for the reabsorption of bile acids, [72] this validated the potential of reuptake of amyloid-beta. In addition, the binding affinity of amyloid-beta with ABCG2, MDR1, and BSEP indicates the possible efflux of amyloid-beta through these receptors.

In addition, we have identified some repurposable drugs that can enhance the expression of the aforementioned genes. The only approved treatment for Alzheimer's disease is the extremely costly monoclonal antibody aducanumab, which compels one to investigate the already-approved repurposable medications for Alzheimer's disease [73]. Anti-tuberculous drug rifampicin, anti-diabetic drug metformin, anti-oxidant resveratrol, and vasodilator cilostazol are our proposed repurposed drugs. We provided empirical evidence from clinical trials that supported the efficacy of these medications in treating AD.

According to the results of our docking investigation, a significant binding affinity exists between rifampicin and the PXR, as well as between 24-hydroxycholesterol and LXR-β. We also found that that administering a PXR agonist to activate the PXR receptor increases the expression of the MDR1/ABCB1 gene. This was accomplished by analyzing gene expression patterns. In the same manner, stimulating the LXR-β receptor with an LXR agonist also raises the levels of ABCA1 and SCD gene expression, as verified with our GEO profile. This contributes to the decrease of amyloid-beta production by lowering the β-cleavage of the amyloid-beta precursor protein[74]. In a separate study, Vats et al. reported that metformin increases the expression of the human bile salt export pump ABCB11 gene, which plays an essential role in increasing the amyloid-beta efflux [75].

Our docking study revealed that both resveratrol and cilostazol exhibit a moderate binding affinity with ASBT and PDE-3, respectively. Resveratrol prevents EHC from occurring by reducing the expression of ASBT, which in turn enhances the clearance of intracellular amyloid-beta through the action of the proteasome [47]. Conversely, Cilostazol is a PDE-3 inhibitor that raises the amount of cAMP, activates protein-kinase-A and stimulates subsequent phosphorylation of cAMP response element-binding protein (CREB). Phosphorylation of CREB is important for initiating the formation of new genes

such as ABCA1 and is also in charge of the production of proteins that are necessary for strengthening synaptic connections [76, 77].

Furthermore, our results of the MD simulation showed that the RMSD values of docked complexes are within the permissible limit of one to three angstroms. In addition, the RMSF values were analyzed to determine whether or not there were fluctuations in the complexes, and we found that these complexes possessed an acceptable level of stability. In addition, by interaction analysis we identified hydrophobic interactions, hydrogen bonds, and the creation of water bridges in the docked complexes. In addition to this, the cilostazol-PDE complex displayed an additional ionic contact, and magnesium ions mediated this interaction.

In addition, our gene ontology and pathway enrichment analysis of the gene expression profile for LXR and PXR activation elucidated the participation of several cellular processes. These analyses were performed on the gene expression profile. Our research revealed that the most prevalent cellular processes are cholesterol efflux, ABC transporters associated with cellular detoxification, cell cycle regulators, and fibrillar collagen trimers. The first cleavage of amyloid-beta precursor protein with beta-secretase enzyme takes place in cholesterol-rich milieu, which suggests that cholesterol efflux might limit amyloid-beta buildup. This was confirmed by a large body of research [78]. In addition, ABC transporters are necessary for amyloid-beta efflux [44, 79, 80] and the results of our investigation demonstrated that activation of LXR and PXR increases the expression of ABC transporters.

Moreover, we demonstrated that monotherapy with a single drug is not a proper option since multidrug combination therapies are required to treat Alzheimer's disease due to its intricate multifaceted pathophysiology. Based on the results of our synergism study, the combination of rifampicin and metformin generates a greater pharmacological impact

than the combination of rifampicin, cilostazol, and metformin does. Since CYP3A4 enzyme is responsible for the metabolism of cilostazol, the presence of rifampicin, which is a powerful inducer of CYP3A4, would result in lower serum concentrations of cilostazol [81, 82]. Hence, it is possible that this process is what caused the triple combination to have a less effective therapeutic impact.

3.5 Conclusion

Our present investigation suggests that the hepatobiliary and entero-hepatic circulation-based transport of amyloid-beta plays a crucial role in increasing the amyloid-beta burden in brain. To ameliorate this, our identified reprofiled drugs, Rifampicin, Resveratrol, Metformin, and Cilostazol, may have capability to increase intestinal – fecal amyloid-beta excretion and reduce amyloid-beta reabsorption by targeting our identified receptors involved in enterohepatic circulation.